Reorientational Dynamics of Poly(vinylidene fluoride)/Poly(methyl methacrylate) Blends by Broad-Band Dielectric Relaxation Spectroscopy

Jo Wing Sy and Jovan Mijovic*

Department of Chemical Engineering, Chemistry and Materials Science, Polytechnic University, Six Metrotech Center, Brooklyn, New York 11201

Received May 4, 1999

ABSTRACT: A comprehensive investigation of the reorientational dynamics of poly(vinylidene fluoride)/poly(methyl methacrylate) (PVDF/PMMA) blends was carried out. Dielectric relaxation spectroscopy (DRS) was performed over 11 decades of frequency and over a wide range of temperature on wholly amorphous, crystalline, and crystallizing blends of varying composition. The range of experimental conditions and compositional variables far exceeded those employed by previous investigators, enabling us to formulate a comprehensive view of the dynamics in these systems. A number of relaxation processes were detected, and their origins, temperature dependence, composition dependence, and spectral characteristics were established. Three α-type processes were observed: the α_a process, associated with relaxations of *all* amorphous PVDF segments (not only within the crystalline−amorphous interphase); the α_m process, which encompasses several relaxation processes and scales with blend composition; and the α_c process, attributed to relaxations within the crystalline phase. With decreasing temperature the α_a process in the blends undergoes a crossover to a localized β_a process, in a manner different from the $\alpha\beta$ splitting observed in many molecular and polymeric glass formers. An explanation of the underlying physics was offered within the framework of an interplay between the physical dimension of various nanoscopic regions in the blend and the characteristic length scale for cooperative relaxation. The $\alpha_a\beta_a$ crossover was shown to be a consequence of the confinement imposed on the amorphous PVDF segments by more rigid PMMA segments and the PVDF crystals.

Introduction

The miscibility and the morphology of blends of poly(vinylidene fluoride) (PVDF) and poly(methyl methacrylate) (PMMA) have been extensively investigated by a variety of techniques that include calorimetric,[1−4] microscopic,[5−7] X-ray,[8−11] dynamic mechanical,[12,13] NMR,[14] FTIR,[14,15] neutron scattering,[16] and dielectric[17,18] measurements. It is now generally agreed that PVDF and PMMA are completely miscible in the melt and exhibit a lower critical solution temperature (LCST) behavior above 300 °C.[6,19] Various proofs of miscibility have been offered, including single DSC T_g, continuous variation in T_g as a function of blend composition, and a negative interaction parameter calculated from SAXS,[2] SANS,[16] melting point depression,[2,20] and inverse gas chromatography.[21]

The morphology of PVDF/PMMA blends depends on the cooling rate and the blend composition; together these parameters determine whether PVDF crystallizes or remains amorphous upon cooling from the melt. Crystalline PVDF/PMMA blends consist of a crystalline PVDF phase and a miscible PVDF/PMMA amorphous phase. The location of the amorphous component is of interest and has been the subject of various studies. Depending on the crystallization conditions, the amorphous component can be (1) located in the interlamellar zone between the crystalline lamellae, (2) excluded from the interlamellar zone but contained within the spherulite, and/or (3) rejected either partially or completely from the spherulite, resulting in the formation of a matrix in which the spherulites are embedded.[22] A number of studies have argued that PMMA is accommodated between the PVDF lamellae—examples include SAXS measurements that show an increase in the thickness of the amorphous region between the crystalline lamellae with increasing PMMA.[8−10] However, the work of Saito and Stühn claims that PMMA could be partially excluded from the interlamellar region at lower crystallization rate.[11]

Morphological investigations of crystalline polymers have assumed a new dimension with the introduction of the concept of interphase. The term interphase was coined in the 1970s, and it is now generally agreed upon that the morphology of crystalline polymers consists of a crystalline lamellar phase, an amorphous phase, and a crystal−amorphous interphase. Experimental and theoretical evidence for the existence of a crystal−amorphous interphase in crystalline homopolymers and polymer blends has been claimed by several authors. The initial argument could be traced to the classic studies by Flory,[23,24] who pointed out that the boundary between the ordered crystals and the disordered liquid-like regions in crystalline polymers cannot be as sharp as in monomeric systems. Since then, a number of theoretical[25−27] and experimental studies[28,29] have been performed, and quantitative descriptions of the interphase have been made. The formation of an interphase in crystalline PVDF/PMMA blends has also been proposed on the basis of theoretical considerations of chain packing at the surface of lamellar crystallites.[30,31] It was argued that the transition from the perfect order in the crystal to the isotropy in the amorphous phase cannot occur abruptly and that PMMA must be excluded from the crystal−amorphous interphase. An interesting experimental study of PEO/PMMA blends by SANS and SAXS was conducted by Russell et al.[32] These authors reported a 1.5 nm discrepancy between the widths of the diffuse-phase boundary as measured by SAXS and

* To whom correspondence should be addressed.

10.1021/ma9907035 CCC: $19.00
Published on Web 01/22/2000

SANS and attributed it to the presence of an interphase devoid of PMMA.

Our interest in this study is focused on the understanding of the dynamics and the molecular origin of relaxations associated with different morphological regions in PVDF/PMMA blends by broad-band dielectric relaxation spectroscopy (DRS). A limited number of dielectric studies of polymer blends have been reported in the literature.[33−46] In recent years, the interpretation of dielectric response in a number of miscible crystalline blends has been aided by the concept of interphase. In addition to PVDF/PMMA,[2,18,41,42] the systems studied include poly(ϵ-caprolactone)/poly(vinyl chloride) (PCL/PVC), poly(ethylene oxide)/poly(methyl methacrylate) (PEO/PMMA), and poly(butylene terephthalate)/polyacrylate (PBT/Par) blends.[34] A relaxation process similar to that in the neat crystalline component was found in all those cases and was associated with the interphase. Interestingly, the relaxation time for this process was found to be dependent on blend composition in PCL/PVC and PBT/Par but independent in PVDF/PMMA and PEO/PMMA blends. Unfortunately, most of these studies were based on the dielectric results obtained from temperature scans that provide only limited fundamental information about the underlying physics.

A brief recap of the fundamental principles of dielectric relaxation spectroscopy (DRS) is offered below. Of the experimental techniques available for the study of reorientational dynamics in molecular liquids, liquid crystals, and polymers, dielectric relaxation spectroscopy (DRS) is rapidly becoming a dominant tool.[47−49] The great potential of DRS derives from an unparalleled frequency range available (12−14 decades) that enables one to probe molecular dynamics of condensed matter in various phases and at different temperature: from amorphous liquids to a liquid crystalline glass; from high temperature, where the dipole relaxation times are of the order of tens of picoseconds, through the vitrification process where the glassy relaxation times reach tens to hundreds of seconds. Dielectric permittivity is related to the dipole moment correlation function by a Fourier transformation:[50]

$$\frac{\epsilon^*(\omega) - \epsilon_\infty}{\epsilon_0 - \epsilon_\infty} = 1 - i\omega\int_0^\infty e^{-i\omega t}\phi(t)\,dt \qquad (1)$$

where ϵ_0 is the limiting low-frequency value of the dielectric constant, ϵ_∞ is the limiting high-frequency dielectric constant, ω is angular frequency, and $\phi(t)$ is the relaxation kernel that can be obtained from the dipole correlation function:

$$\phi(t) = \frac{\sum_i^N\sum_j^N \langle \mu_i(0)\cdot\mu_j(t)\rangle}{\sum_i^N\sum_j^N \langle \mu_i(0)\cdot\mu_j(0)\rangle} \qquad (2)$$

where $\mu_i(0)$ and $\mu_j(t)$ denote the elementary dipole moment of molecules i and j at time $t = 0$ and t, respectively. The correlation function expressed in this form takes into account both equilibrium and dynamic angular correlations between molecules. The relaxation kernel, $\phi(t)$, is most often quantified via a stretched exponential function of the Kohlrausch−Williams−Watts[51] (KWW) type:

$$\phi(t) = Ce^{-(t/\tau)^\beta} \qquad (3)$$

where C is a constant, τ is the relaxation time, and β is the stretching exponent ranging form 0 to 1. It is sufficient to use only one portion of the real or imaginary permittivity in eq 1, since they are related by the Kramers−Kronig transform, and then by taking the imaginary part of the Fourier transform of eq 2, we obtain

$$\phi(t) = \frac{2}{\pi}\int_0^\infty \frac{\epsilon''(\omega)}{\epsilon_0 - \epsilon_\infty}\frac{\cos(\omega t)}{\omega}\,d\omega \qquad (4)$$

However, instead of transforming the frequency domain dielectric data into the time domain using a discrete Fourier transform, where spectral features may be truncated, we transform the relaxation kernel $\phi(t)$ into the frequency domain, using the technique described by Dishon et al.[52] and then fit the experimental data to the transformed kernel with appropriate parameters. Alternatively, ϵ^* may be modeled by a number of empirical functions; a particularly popular and robust form is the Havriliak−Negami[53] (HN) function given as

$$\epsilon^*(\omega) = \epsilon_\infty + \frac{\epsilon_0 - \epsilon_\infty}{[1 + (i\omega\tau_{HN})^a]^b} + i\frac{\sigma}{\omega^n\epsilon_v} \qquad (5)$$

where a and b are the dispersion shape parameters, σ is the conductivity, n accounts for deviations in the migrating charge mechanisms, ϵ_v is the vacuum permittivity, and the other parameters are defined in eq 1.

The measured dielectric permittivity (ϵ^*) thus contains information that is unique to the molecular-level composition of the material. The interpretation of the polarization response, because the energy changes involved in the various polarization mechanisms are widely distributed and the values of $h\omega/kT$ are low, does not require a quantum mechanical treatment and can proceed from classical electromagnetic theory.

The principal objective of this study was to provide a comprehensive view of dipole dynamics in PVDF/PMMA blends. This was accomplished by performing dielectric relaxation spectroscopy (DRS) in the frequency domain on a series of blends of different composition and morphology (wholly amorphous, crystalline, crystallizing) and over a range of frequency (11 decades) and temperature that far exceed those used by previous investigators.

Experimental Section

Materials. PMMA was Plexigalass VS-100 from Rohm and Haas. The average number molecular weight is about 67 000 g/mol. PVDF was Kynar 721 from Pennwalt. The blends ranging from 0 to 100 wt % PMMA were prepared at 10% intervals in a twin-screw extruder (Werner-Pfleiderer). *The blend composition is defined throughout the text as X/Y, where X and Y represent the weight percent of PVDF and PMMA, respectively.*

Techniques. The principal experimental tool was dielectric relaxation spectroscopy (DRS). Our facility for dielectric measurements consists of modified commercial and custom-made instruments that include (1) Solartron 1260 impedance gain phase analyzer (10 μHz−32 MHz), (2) Hewlett-Packard 4284A precision LCR meter (20 Hz−1 MHz), (3) Hewlett-Packard 8752 A network analyzer (300 kHz−1.3 GHz), and (4) Hewlett-Packard 4291 A rf impedance analyzer (1 MHz−1.8 GHz). All instruments are interfaced to computers via IEEE 488.2 and equipped with heating/cooling capabilities,

Table 1. Summary of Characteristic Transitions and Degree of Crystallinity as a Function of Blend Composition

blend omposition	T_g[a] (°C)	T_g[b] (°C)	T_m[b] (°C)	T_c[c] (°C)	X_c[b] (%)
neat PVDF		−39	172	136	59.5
90/10			172	134	57
80/20		44	168	128	52.6
60/40	33	68	166	94	51
50/50 blend	48	70	164		41.9
20/80	88				
PMMA	105				

[a] T_g for amorphous samples was measured by differential scanning calorimetry at a heating rate of 10 °C/min. Both 60/40 and 50/50 blends were rendered amorphous by quenching from melt to liquid nitrogen. [b] T_g and T_m for crystalline samples were measured by differential scanning calorimetry at a heating rate of 10 °C/min. Crystalline samples were prepared as follows: (1) heat to 200 °C and maintain for 20 min to melt all crystals; (2) anneal. Annealing temperature and time for different blends are the following: PVDF, 90/10 and 80/20 blends: 10 h at 155 °C; 60/40 blend: 15 h at 145 °C; 50/50 blend: 50 h at 145 °C. The degree of crystallinity, X_c, is calculated from the ratio of the specific heat of fusion of PVDF in the blend and the heat of fusion estimated for 100% crystalline PVDF, 25 cal/g.[56] [c] Crystallization temperature is determined by cooling from 200 °C at 10 °C/min.

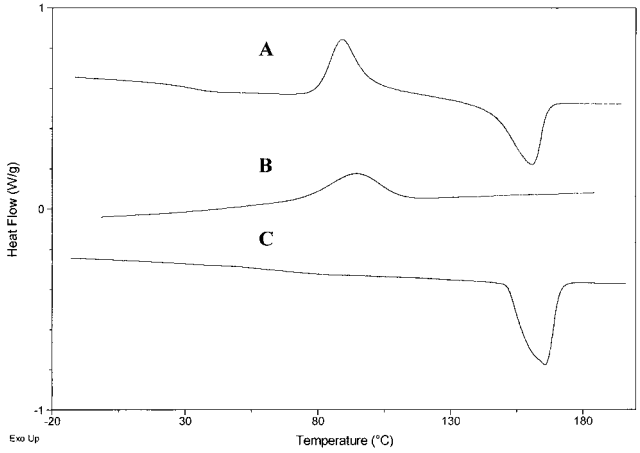

Figure 1. DSC thermograms of 60/40 blend: (A) heating following quench; (B) cooling from the melt; (C) heating following anneal.

including Novocontrol's Novocool system. A variety of sample cells and accessories were used including low-frequency parallel plate configuration, high-frequency cell in conjunction with high-precision extension airline, a cell for simultaneous DSR/remote fiber-optic FTIR tests, etc. Further details can be found in our recent publications.[54,55] Supporting evidence was obtained from differential scanning calorimetry (DSC), FTIR, and optical microscopy.

Experimental Strategy. The dielectric response of blends with varying compositions was studied in three different morphological states: wholly amorphous, crystalline, and crystallizing (i.e., during crystallization). A companion DSC and FTIR study was performed to obtain supplementary information about morphology, degree of crystallinity, glass transition temperature, and melting temperature to ensure that the samples studied by DRS are well-defined. DSC results for all blends are summarized in Table 1. Figure 1 shows a set of thermograms for a 60/40 PVDF/PMMA blend. Glass transition, crystallization, and melting are clearly seen in curve A, which was obtained during heating following the quench into liquid nitrogen from the melt. The enthalpy of crystallization and melting was identical (within the experimental error), indicating that the sample was initially wholly amorphous. The crystallization temperature was determined by the cooling run (curve B). Note that the crystallization temperature decreases considerably with increasing PMMA content. The thermogram of the crystalline sample is shown in curve C, from which the melting point was read. The degree of crystallinity, X_c, is calculated from the ratio of the specific heat of fusion of PVDF in the blend and the heat of fusion estimated for 100% crystalline PVDF.[56] FTIR measurements were performed to ensure that the blends were amorphous after quenching. FTIR spectra for the 60/40 blend shown in Figure 2 provide a good example. The upside-down look of Figure 2 is caused by the strong absorption in the 1600−1000 cm^{-1} range of the mid-infrared spectrum, which is not shown here. Our goal here was merely to accentuate the difference in the characteristic peaks in the 400−800 cm^{-1} range. Five characteristic absorption peaks due to the PVDF crystal form II,[41,57] at 410, 531, 613, 766, and 796 cm^{-1}, are clearly seen in curve C which represents a crystalline sample annealed at 57 °C for 7 h. These peaks are absent in curve A (quenched and hence wholly amorphous sample) and are gradually developing in curve B (sample annealed for 15 min).

Results

The presentation of the results is subdivided into three parts. In sections one and two we describe the dynamics of crystalline and wholly amorphous blends, respectively. In the third section we offer an in-situ real-time look at dipole dynamics *during* isothermal crystallization.

1. Crystalline PVDF and PVDF/PMMA Blends. Although this study is focused on blends, a recap of the dielectric response of the individual components, PVDF and PMMA, is in order. Early studies of the relaxation processes in PVDF and PMMA can be found in the literature.[58−62] Three relaxation processes are observed in crystalline PVDF: (1) the α_a process, due to segmental motions in the amorphous phase; (2) the α_c process, associated with the crystalline phase;[59,63−65] and (3) the β process, caused by localized motions. Figure 3A shows dielectric loss in the frequency domain (10 decades) for crystalline PVDF at a series of temperatures. Both α_a and α_c processes are clearly visible, and their temperature dependencies are beautifully discerned in Figure 3A. A weak and broad β process is detected at low temperatures, as seen in Figure 3B. Careful inspection of Figure 3B reveals how a decrease in temperature from −41 to −100 °C causes the β process to evolve from the high-frequency (fast) end of the α_a process into a separate process. Frequency sweeps at different temperatures are used to construct the relaxation maps for the α_a, the α_c, and the β process in crystalline PVDF. These results are shown in Figure 4, together with the results for blends. Figure 4 is busy but comprehensive, and we shall revert to it repeatedly throughout the text. For the moment, however, we focus attention on the α_a process in neat PVDF, which is represented by open circles in Figure 4. It is interesting to note that the temperature dependence of this process cannot be fitted by a single Vogel−Fulcher−Tammann (VFT) equation, although the observed curvature is similar to the response commonly found in molecular and polymeric glass formers. The α_c and the β process in neat PVDF are Arrhenius-like, with an activation energy of 22 and 10.5 kcal/mol, respectively.

Relaxation dynamics of neat PMMA, the other component in the blend, are described next. It should be immediately stressed that the composition and the tacticity of commercial grades of PMMA vary with the source, resulting in different physical/mechanical properties that are not readily comparable. Consequently, our goal here is not to be comprehensive but to identify the various relaxation processes in the PMMA used in

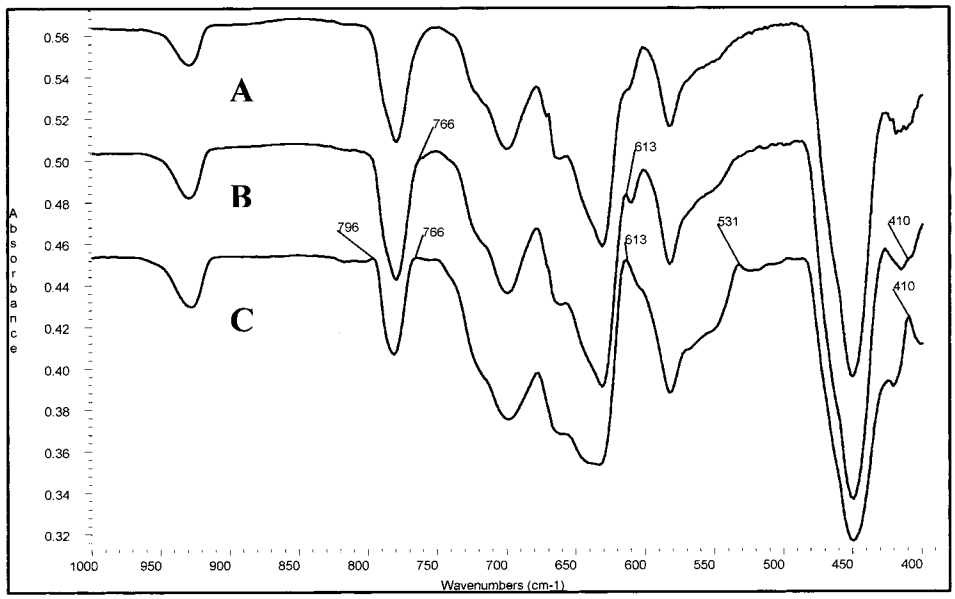

Figure 2. FTIR spectra of 60/40 blend: (A) quenched; (B) annealed at 57 °C for 15 min; (C) annealed at 57 °C for 7 h.

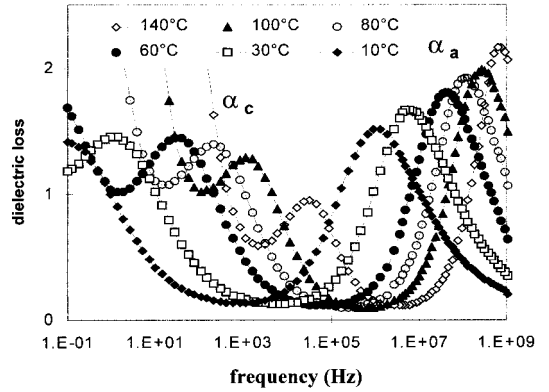

(A)

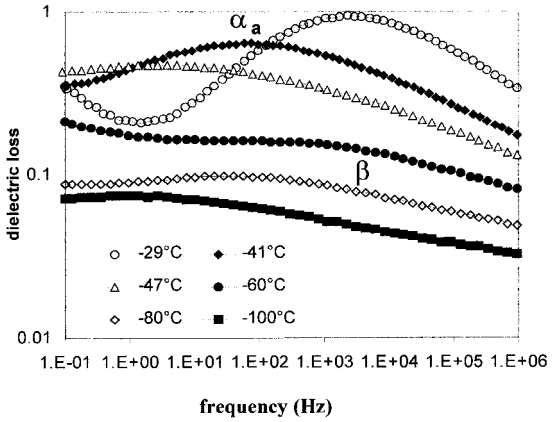

(B)

Figure 3. Dielectric loss in the frequency domain with temperature as a parameter for crystalline PVDF: (A) 10 to 140 °C; (B) −29 to −100 °C.

this study as a necessary prerequisite for the development of an understanding of its dielectric behavior in blends. Dielectric loss in the frequency domain (11 decades), below and above the DSC T_g of PMMA (ca. 105 °C), is shown in Figure 5. A strong β process, associated with the localized motions of side groups in the glassy state, is found below the T_g. The intensity of

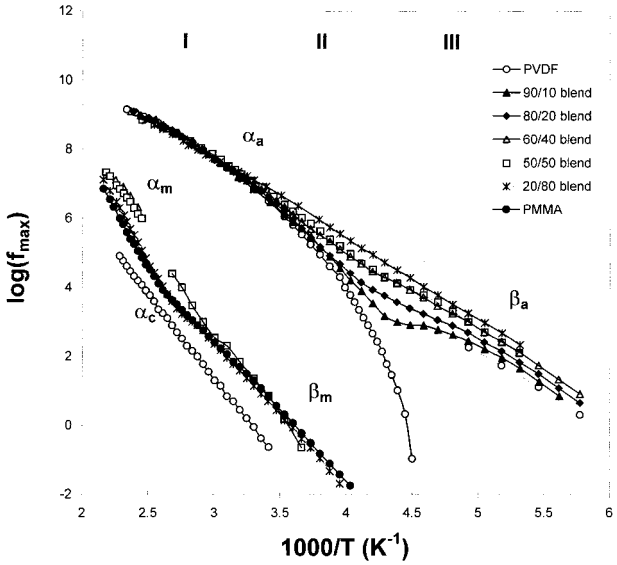

Figure 4. Frequency at maximum loss as a function of reciprocal temperature for various relaxations in PVDF, PMMA, and PVDF/PMMA blends of different composition.

β relaxation increases with increasing temperature. Eventually the β process merges with the α process (associated with segmental motions) to give rise to $\alpha\beta$ relaxation which is present around and above the T_g. Although a separate α relaxation cannot be clearly seen in Figure 5 because of the high conductivity that dominates the dielectric response at low frequency, an unmistakable signature of its presence is the observed increase (plateau) in loss intensity at the high end of the conductivity tail between 100 and 120 °C (see arrow in Figure 5). Above 120 °C, however, the α process shifts quickly across the frequency window of Figure 5, and already at 150 °C a single $\alpha\beta$ process is observed. Inspection of the temperature dependence of $\alpha\beta$ and β processes in PMMA (filled circles in Figure 4) clearly reveals a crossover from β to $\alpha\beta$ relaxation with increasing temperature. An Arrhenius-like β process, with activation energy of 19 kcal/mol, is replaced by the $\alpha\beta$ process around T_g, as evidenced by the abrupt change in the slope.

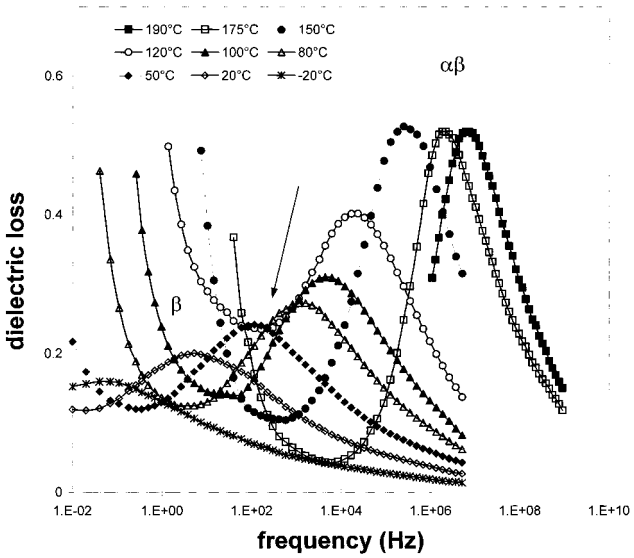

Figure 5. Dielectric loss in the frequency domain with temperature as a parameter for neat PMMA.

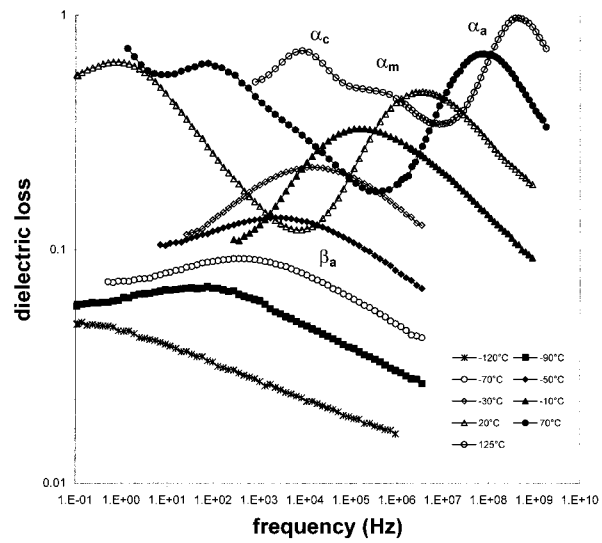

Figure 6. Dielectric loss in the frequency domain with temperature as a parameter for crystalline 80/20 blend.

Crystalline blends were examined next: their dielectric response was very interesting, and a number of relaxation processes were observed. Previous investigations have shown that a relaxation similar to the α_a process in neat PVDF was also present in crystalline and amorphous PVDF/PMMA blends. Since this relaxation was also observed in our blends, we shall refer to it as the α_a process. What other relaxation processes exist in the blends? An answer to that question is contained in Figure 6, which shows dielectric loss in the frequency domain with temperature as a parameter for a crystalline 80/20 blend. Three α-type relaxation processes are clearly identified at 125 °C (open circle) in Figure 6: these are, in the order of increasing frequency, α_c, α_m, and α_a. The intensity and location of these relaxations depend, to a varying degree, on blend composition, as will be described later. Localized motions observed in neat PVDF (Figure 3B) and neat PMMA (Figure 5) are also present in the blends and are referred to as β_a and β_m relaxation, respectively. A partial overlap of α_c and α_m relaxations, seen in Figure 6 at 125 °C, becomes more pronounced with increasing PMMA content and decreasing temperature, making deconvolution of these processes arbitrary and physically meaningless. This is clearly demonstrated by comparing the loss curves at 125, 70, 20 °C (Figure 6). The α_a process, on the other hand, is well separated from other processes over a wide range of frequency and temperature and can be analyzed with confidence. We now revisit Figure 4 and examine the temperature dependence of α_a and β_a processes in crystalline blends of different composition. To facilitate the description and interpretation of our results, we divide Figure 4 into three regions, labeled I−III. It is immediately clear that the data for neat PVDF and for all blends fall on top of each other in region I (above ca. 20 °C) and that the most probable relaxation time for the α_a process is independent of blend composition in that temperature range. In region II (below 20 °C and above −50 °C), however, a typical curvature associated with glass formation, which is clearly seen in neat PVDF, is absent in the blends. Instead, we note a gradual crossover from segmental to localized motions (α_a to β_a relaxation) with decreasing temperature—an interesting observation that has not been reported hitherto in the literature. We emphasize that this is not a case of the commonly observed $\alpha\beta$ splitting, where these two processes diverge but maintain identity with decreasing temperature; here the α process ceases to exist (see Figure 6). The underlying physics is described later in the text. For the moment we note that the most probable relaxation time decreases with increasing PMMA content and that the divergence of curves in region II of Figure 4 is enhanced with decreasing temperature. Region III in Figure 4 represents the glassy state and is characterized by an Arrhenius-like temperature dependence of β_a relaxation in all samples. Although the activation energy for the β_a process is independent of blend composition (constant slope), the curves shift upward, (i.e., faster relaxation) with increasing PMMA content.

We now briefly address the issue of the molecular origin of the α_a process in PVDF/PMMA blends, as a prelude to an explanation of the observed crossover from α_a to β_a relaxation. It was proposed that the α_a process in PVDF/PMMA blends originates within the crystalline−amorphous interphase.[2,17] The exclusion of PMMA from the interphase leaves an almost pure PVDF phase whose composition does not depend on the degree of crystallinity or the composition of the miscible phase. This concept is supported by experimental observations in other semicrystalline blends, including PEO/PMMA, PCL/PVC, and PBT/Par,[32,34] where a relaxation similar to that in the neat crystallizable component was observed. However, our current findings suggest a more complex molecular origin of the α_a process, and that has prompted us to revisit the earlier concepts about the interplay between the reorientational dynamics of dipoles and morphology in PVDF/PMMA blends. Whereas we have no qualms with the morphological picture that includes an amorphous interphase in crystalline polymers—a physically meaningful concept—there is definitive evidence from DRS in support of the idea that the α_a process in our system occurs in the *entire amorphous phase* of the PVDF component and cannot be attributed exclusively to the interphase. Crucial evidence about the origin of the α_a process was obtained from the dielectric measurements of wholly amorphous blends, and these results are presented next.

2. Wholly Amorphous Blends. Experimental strategy for the study of wholly amorphous blends was based

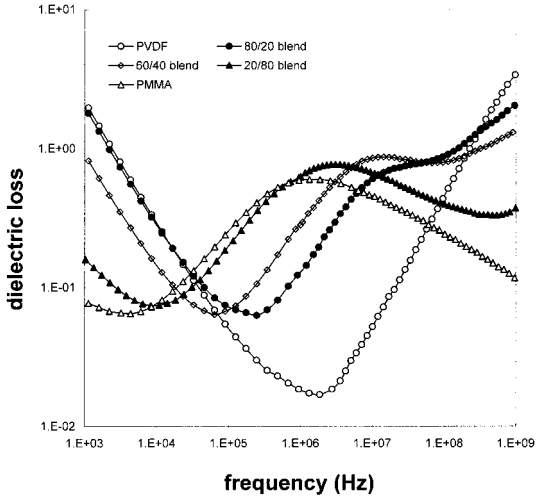

Figure 7. Dielectric loss in the frequency domain at 170 °C for PVDF/PMMA blends with composition as a parameter.

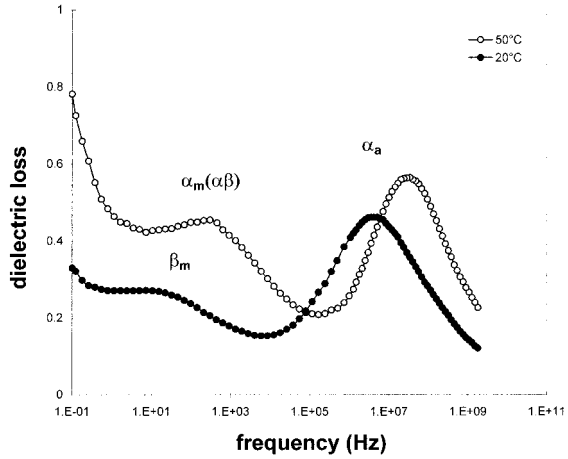

Figure 8. Dielectric loss in the frequency domain at two selected temperature for wholly amorphous 60/40 blend.

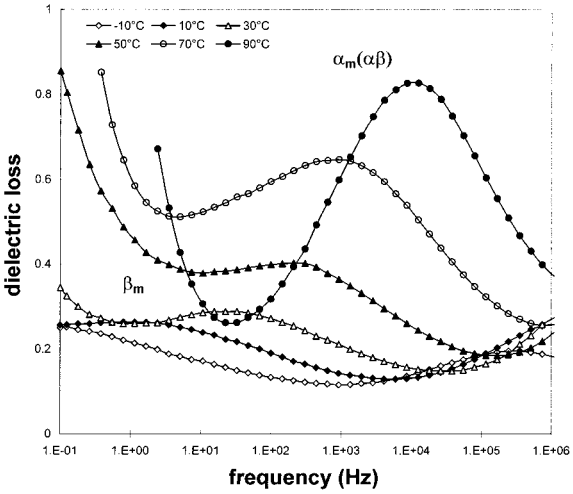

Figure 9. Dielectric loss in the frequency domain with temperature as a parameter for wholly amorphous 50/50 blend.

on frequency sweeps of samples rendered amorphous via two different thermal histories: (1) blends in the amorphous melt at a selected temperature before the onset of crystallization and (2) blends quenched (into liquid nitrogen) and swept at a selected temperature where no crystallization took place. We first consider samples that were melted and then tested at a temperature in the vicinity of T_m, where the rate of crystallization was zero or largely negligible in comparison with the time scale of the dielectric measurements. One such example is shown in Figure 7, which contains dielectric loss in the frequency domain for different blend compositions at 170 °C. Neat PMMA and PVDF were swept first, and a single relaxation process (α) was found in each polymer. The loss peak maximum was located at about 2 MHz for PMMA and above 1 GHz for PVDF. On the basis of the presumed complete miscibility of PVDF and PMMA over the entire composition range, it was anticipated that a single α process would be also observed in all amorphous blends at high temperature (above T_m), but that was not found. Instead, we observed two relaxation processes in all blends in the melt (amorphous) state: a slow process, α_m, and a fast one, α_a. Inspection of Figure 7 reveals clearly that the α_m process depends on blend composition and shifts to higher frequency with increasing amount of PVDF, while the α_a process remains unaffected by the change in blend composition. This result, which has not been reported hitherto in the literature, must be interpreted *as unambiguous evidence that the* α_a *process cannot be associated exclusively with the amorphous−crystalline interphase, simply because the crystalline phase is absent in the melt*. Further support for this tenet comes from the dielectric measurements of 60/40 and 50/50 blends that were exposed to a different thermal history and were rendered wholly amorphous by quenching from above the melting point into liquid nitrogen. Figure 8 shows dielectric loss in the frequency domain for a 60/40 blend quenched and then tested at 20 and 50 °C, i.e., below and above the calorimetric (DSC) T_g of that blend (about 33 °C). It is clearly seen that the α_a process persists below and above the DSC T_g, although its intensity drops with decreasing temperature. The slow α_m process, seen in Figure 8 at 50 °C, is broad and of irregular shape, indicating a complex relaxation mechanism that encompasses localized (β_m type) motions in PMMA, coupled with the combined segmental (α type) motions of PMMA segments and a portion of PVDF segments not engaged in the α_a process. We shall describe later in the text how the length scale for cooperative relaxations of PVDF segments dictates their distribution between α_m and α_a processes. Below the calorimetric T_g (20 °C sweep, Figure 8), only the β_m process is observed. We have already described a strong β process and the crossover from β to $\alpha\beta$ mechanism with increasing temperature in neat PMMA; it is now of interest to establish what happens in the blends, i.e., how the presence of PVDF affects this crossover.

We ask two important questions: (1) how is the β_m process in PMMA influenced by the gradual addition of PVDF, and (2) how is the α_m process in a blend different from the $\alpha\beta$ process in neat PMMA? An attempt to answer these questions is made by inspecting the dielectric response of a quenched (wholly amorphous) 50/50 blend, whose dielectric loss in the frequency domain at several selected temperatures is shown in Figure 9. An important characteristic of this blend is that it remains wholly amorphous during frequency sweeps at temperatures as high as 40 °C above its DSC T_g (about 48 °C). A broad relaxation process, labeled β_m in Figure 9, is noted in the glassy state. This process is associated with the localized motions of PMMA segments. A further increase in temperature is accompanied by a slow emergence of the α_m process, which is broad and skewed at low frequency, as readily seen by

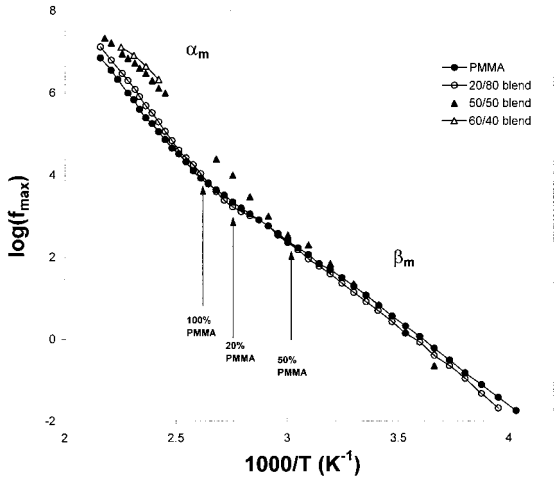

Figure 10. Frequency at maximum loss as a function of reciprocal temperature for α_m and β_m relaxations in PMMA and wholly amorphous blends of different composition.

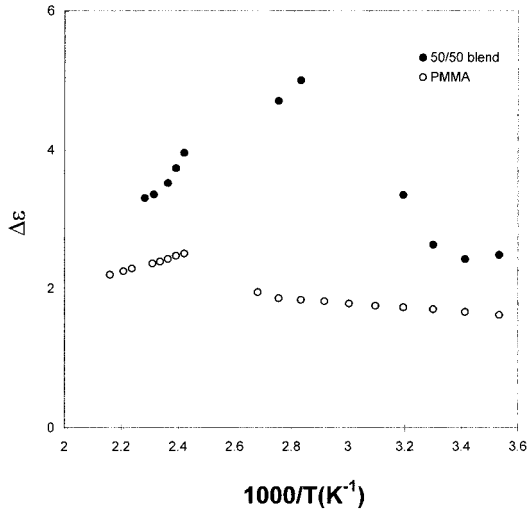

Figure 11. Dielectric relaxation strength as a function of reciprocal temperature for PMMA and wholly amorphous 50/50 blend.

examining the loss curves at 50 and 70 °C in Figure 9. This parallels the trend observed in neat PMMA, the principal difference being that the α_m process in the blends also includes a portion of PVDF segments. The intensity of the loss peak increases considerably with increasing temperature, and at 90 °C, β_m and α_m processes merge to give rise to a single process. It is also interesting to note that the overlap of these relaxation mechanisms is more apparent in blends than in neat PMMA (contrast Figures 5 and 9). An explanation of the physics that underlies this observation is provided in the Discussion section.

The observed β_m to $\alpha\beta$ crossover is readily seen in the relaxation map. The temperature dependence of α_m and β_m processes (already included in the composite plot of Figure 4) is replotted for clarity in Figure 10. Data for neat PMMA and a 20/80 blend (noncrystallizable), given as reference, are continuous over the entire temperature range because both samples are wholly amorphous under all conditions. The gaps in the data for 60/40 and 50/50 blends correspond to the temperature range where crystallization during the sweep cannot be neglected. The α_m to β_m crossover is readily detected by inspection of Figure 10. Note that data for all samples show two slopes and that each persists over a wide temperature range. The temperature onset of α_m to β_m crossover, marked by arrows in Figure 10, decreases with increasing PVDF content because the crossover represents the dielectric glass transition, and it shifts to lower temperature with increasing amount of the low-T_g component, i.e., PVDF. This is further supported by data in Figure 11, where relaxation strength is plotted as a function of reciprocal temperature for neat PMMA and a quenched 50/50 blend. The relaxation strength of neat PMMA increases slightly with temperature in the glassy state where segmental motions are frozen and the β_m process dominates the dynamics. The activation of segmental motions in the glass transition range leads to a stepwise increase in the relaxation strength, $\Delta\epsilon$. Although the presence of a step in $\Delta\epsilon$ is beyond doubt, no points were included in that range because data could not be fit to a single HN equation. The inverse proportionality between the relaxation strength and temperature observed above T_g is a common characteristic of amorphous glass formers. The response of a quenched 50/50 blend differs from neat PMMA in that the stepwise increase in relaxation strength is shifted to lower temperature and is more pronounced. A gap in the data above T_g (Figure 11) corresponds to the temperature range in which crystallization during measurement cannot be neglected. A decrease in temperature at which the stepwise change in $\Delta\epsilon$ occurs is not surprising and can be readily attributed to a decrease in T_g caused by the addition of PVDF. The observed increase in the magnitude of $\Delta\epsilon$ is explained as follows. The α_m process in blends, as stated before, encompasses the localized motions of PMMA segments (β_m) and the combined segmental motions (α-type) of PMMA segments and a portion of PVDF segments. The addition of PVDF augments the total relaxation strength, enhances the α_m process, and leads to a more pronounced crossover. This is clearly seen by comparing the results for neat PMMA and a 50/50 blend at a temperature that bears the same distance from the T_g of each system. Compare, for example, data at 120 °C in Figure 5 with data at 70 °C in Figure 9.

Two more features in Figure 10 are worth pointing out. First, the β_m process in blends of different composition is similar but not identical; the shift in the relaxation time to lower frequency with increasing PVDF content is small but detectable. This parallels the earlier observation for the β_a process (see Figure 4) and is a consequence of the effect of α relaxation on β relaxation. And second, all curves shown in Figure 10 merge at high temperature, independent of blend compositions. The influence of the α process on the β process increases with increasing PVDF content because of a decrease in T_g and an increase in the intensity of α relaxation. (We are currently continuing this investigation.)

3. Isothermal Crystallization. Since the molecular origin of a relaxation process is related to its morphological milieu, it was anticipated that much could be learned about different relaxation processes by monitoring their appearance and/or disappearance *during* crystallization. This goal was pursued and accomplished by conducting in-situ real-time dielectric measurements on a series of crystallizable blends during melt and cold crystallization. The results obtained during melt crystallization are examined first. Figure 12 shows dielectric loss in the frequency domain at different times during crystallization of a 60/40 blend at 137 °C. It should be pointed out here that the loss spectra recorded in each

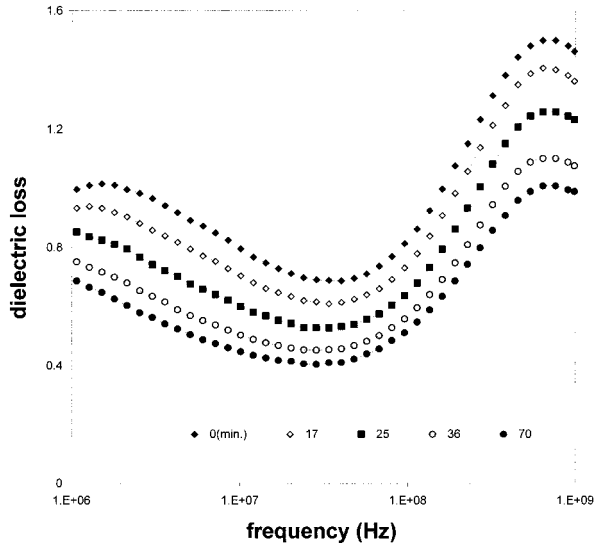

Figure 12. Dielectric loss (α_a) in the frequency domain with time as a parameter during crystallization of a 60/40 blend at 137 °C.

sweep are representative of an isostructure at a different stage of crystallization, because the time scale for a sweep is short (about 40 s) in comparison with the time scale for crystallization at this temperature. The two previously described relaxations, α_a and α_m, are clearly seen in the supercooled liquid prior to the onset of crystallization (see data for $t = 0$, Figure 12). Once the crystallization begins, however, the intensity of the α_a peak decreases steadily but its location stays the same, suggesting that neither the change in the composition of the amorphous phase (as PVDF crystallizes out) nor the appearance of newly formed crystals affects the most probable relaxation time for the α_a process. On the other hand, α_m relaxation shifts to lower frequency with increasing crystallization time. To facilitate the visualization of the development of crystals, we show in Figure 13 a series of optical micrographs taken at different times during crystallization at the same condition of Figure 12 (i.e., 137 °C). Note the gradual development and growth of the spherulitic morphology. The evolution of the α_m process during crystallization of a 60/40 blend at 145 °C is singled out in Figure 14. For clarity, the frequency window of Figure 14 is selected to contain initially ($t = 0$) only α_m relaxation (α_a at $t = 0$ is located at higher frequency, see Figure 12). Crystallization is accompanied by a shift of the composition-dependent α_m relaxation to lower frequency (as PVDF crystallizes out) and the emergence of α_c relaxation: both events are readily observed in Figure 14. The α_c process, which develops during crystallization, is associated with the crystalline phase and was described earlier. A broad dispersion due to the overlapping α_m and α_c processes is noted after crystallization (see e.g. $t = 280$ min, Figure 14).

Equally interesting results were obtained during cold crystallization. This is exemplified in Figure 15, which contains dielectric loss in the frequency domain for a 60/40 blend during cold crystallization at 57 °C. As in the case of melt crystallization, we find that the intensity of the α_a process decreases, but the relaxation time (note the location of maximum loss in Figure 15) remains unchanged during cold crystallization. Moreover, the shape of the loss spectrum does not vary during crystallization, as shown in Figure 16, where normalized loss spectra at different crystallization times are seen to fall on a single master curve. Although we made no further attempts here to study the kinetics of crystallization, the kind of data shown in Figure 15 could be used to that end as demonstrated in an excellent recent study by Williams and co-workers.[66]

We therefore conclude that the DRS results obtained during isothermal (melt and cold) crystallization provide overwhelming evidence that neither the change in the composition of the amorphous phase (as PVDF crystallizes out) nor the formation of crystals affect the relaxation rate of the α_a process. This finding is in complete agreement with the results obtained on crystalline blends, where the change in the amount of amorphous phase was imparted by the change in blend composition. But what physics underlies the relaxation dynamics in the blends? An answer to that question, offered below, is based on the interplay between the length scale of cooperative motions, temperature, and the actual (physical) size of the region within which a relaxation takes place.

Discussion

It is well-known (Adam-Gibbs) that the dynamics in the amorphous phase vary with temperature and that the cooperative length scale for the α process in glass formers increases with decreasing temperature. Of relevance here is what happens in a complex system that consists of two components with different calorimetric T_g's (ca. 105 °C for PMMA and ca. −40 °C for PVDF) believed to be miscible (single DSC T_g) in the amorphous phase at all compositions.

The scenario we propose is one of a system that is globally homogeneous (or miscible, as defined by a single calorimetric T_g) but locally heterogeneous. The length scale of heterogeneities probed by DRS in this study is estimated to be, in the limit, of the order of nanometers, and hence we use the term *nanoheterogeneities*. The existence of nanoheterogeneities in macroscopically homogeneous blends and copolymers is not new and has been supported by the results from diverse experimental techniques that include NMR, DRS, and depolarized light scattering. In an early work, Kwei et al.[67] studied miscible poly(styrene)/poly(vinyl methyl ether), PS/PVME, blends by pulsed NMR and suggested that these systems were not completely homogeneous; they argued that PVME and PS chains were "exclusively mixed" but not "completely mixed" on the segmental scale. An investigation of PS/PVME blends was also carried out by Schmidt-Rohr et al.[68] using two-dimensional wide-line-separation NMR spectroscopy. They reported the existence of nanoheterogeneities with different mobility and estimated a characteristic size of about 3.5 ± 1.5 nm in a 50/50 PS/PVME blend at 320 K. These observations have provoked the obvious question of the physical origin of nanoheterogeneities in globally homogeneous blends, and two schools of thought have emerged in an attempt to supply the answer.

One explanation is that *concentration fluctuations* in globally miscible blends give rise to dynamic nanoheterogeneous environments. A good starting point here is the model proposed by Fischer and Zetsche[69] that can describe the effect of concentration fluctuations in mixtures on the shape of the relaxation spectrum near the glass transition. Katana et al.[37] used this approach to describe the shape of the dielectric α process in the one-phase region of poly(styrene)/poly(cyclohexyl acry-

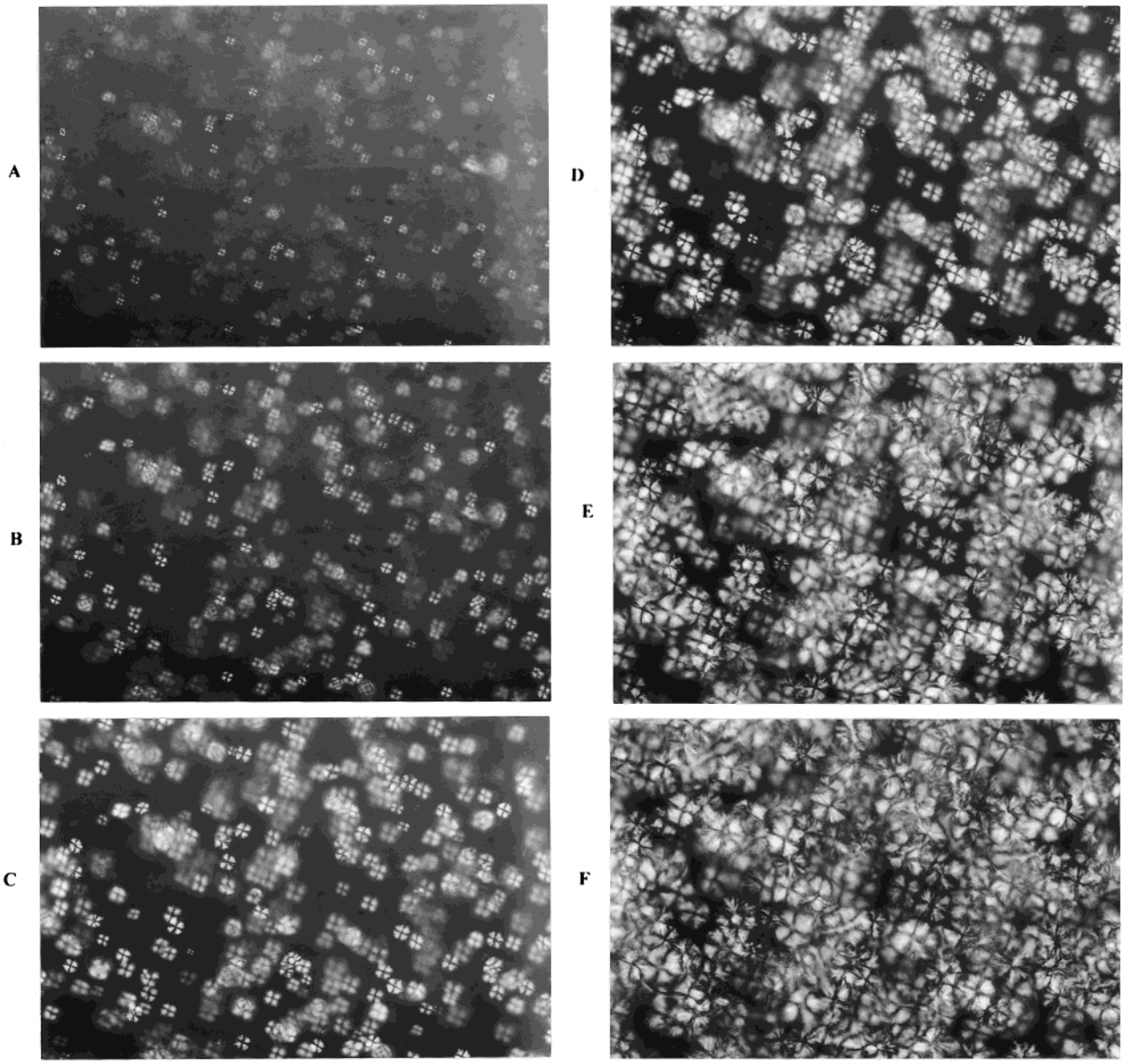

Figure 13. Polarized optical micrographs of 60/40 blend during crystallization at 137 °C: (A) 10, (B) 17, (C) 26, (D) 32, (E) 50, and (F) 70 min.

late-*stat*-butyl methacrylate), PS/P(CHA-*stat*-BMA), blends. They reported that the mean-square concentration fluctuations in this blend could be correlated to the length scale of cooperativity governing the relaxation process near the T_g. A different approach based on coupling model was used by Roland and Ngai[36] to analyze the dielectric dispersion near T_g in PVME/PS blends. They argued that the cooperativity of the local segmental motion in the mixture is determined not only by the nature of the relaxing species but also by the local environment which varies as a function of concentration fluctuations. These fluctuations effectively produce the distributed coupling parameter of each component, which describes the broadening of the glass transition in the blends. More recently, building upon the work of Fischer et al., Kumar[43] and his colleagues proposed a model based on concentration fluctuations that could predict, in some cases, the presence of two distinct microenvironments in globally homogeneous blends. In departure from Fischer's approach, Kumar et al. maintain that a dynamic technique does not probe over a constant length scale but over one that varies with the local composition. For blends of polymers with significantly different T_g's, Kumar's model predicts the existence of two dynamically distinct regions: one with the mobility equal to that of the neat lower T_g component and the other with the average blend mobility.

On the other hand, Khokhlov and Erukhimovich[70] envision the presence of nanoheterogeneities as a consequence of *microphase separation*. They have derived a model based on a significant nonlocal entropic contribution to miscibility that establishes the feasibility of the formation of nanoheterogeneities via microphase separation.

Therefore, it is fair to say that despite the agreement about the existence and the length scale of nanoheterogeneities in miscible blends, the molecular origin and the mechanism associated with this phenomenon remain controversial. It is debated whether nanoheterogeneities result from concentration fluctuations or microphase separation, it is not clear to what extent the dynamics of blend components are affected by mixing, and in our opinion, there is a paucity of reliable data obtained over a wide range of composition and experi-

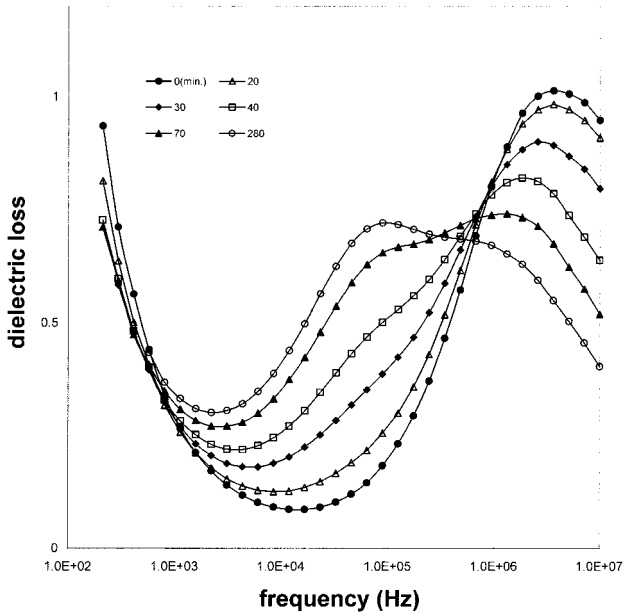

Figure 14. Dielectric loss (α_a and α_c) in the frequency domain with time as a parameter during crystallization of a 60/40 blend at 145 °C.

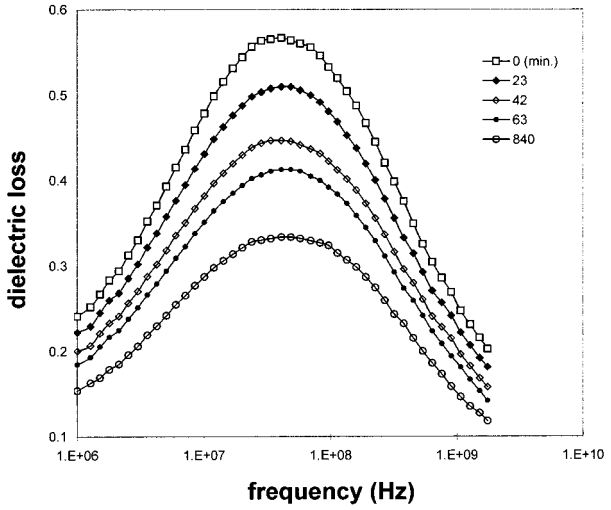

Figure 15. Dielectric loss (α_a) in the frequency domain with time as a parameter during cold crystallization of a 60/40 blend at 57 °C.

mental conditions (particularly in the frequency domain) that would corroborate the model predictions. We raise these points neither as criticisms nor endorsements, only as observations.

The discussion that follows is built as an attempt to consolidate all experimentally observed relaxation processes in PVDF/PMMA blends (see Results) in an effort to interpret the dynamics within the framework of cooperativity. The principal outcome is a comprehensive and largely novel phenomenological description of the physics that underlies the relaxation dynamics of these systems. The presence of nanoheterogeneities is an essential element of our interpretation of the dynamics of PVDF/PMMA blends, and the wealth of information presented here should prove useful to the proponents of models based on concentration fluctuations and microphase separation.

A schematic representation of the interplay between the physical dimension (PD) of each nanoscopic region, the length scale for the cooperative rearranging region

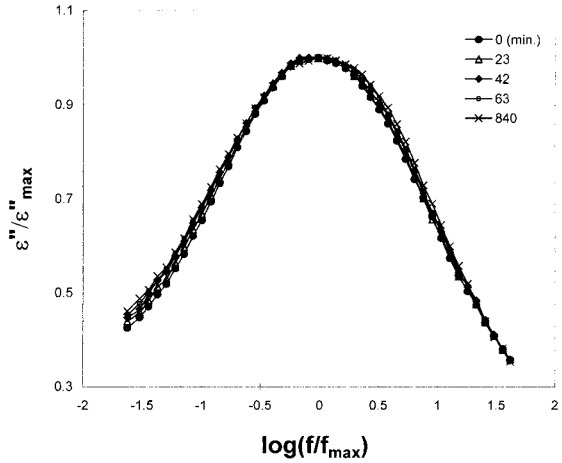

Figure 16. Normalized loss spectra at selected times during cold crystallization of a 60/40 blend at 57 °C.

(CRR), and temperature is shown in Figure 17, which is designed to aid our interpretation visually. It is obvious that relaxation phenomena are bound to be more complex in polymer blends than in homopolymers and/or molecular liquids, though the underlying principle of cooperative motions is common to all these systems. Figure 17 zeroes in on a representative amorphous portion of a PVDF (white areas)/PMMA (black areas) blend that is globally homogeneous but locally nanoheterogeneous. The principal dynamic characteristic of a CRR within which relaxations take place is the length scale for these motions. In Figure 17A−D, we show schematically how a decrease in temperature affects the length scale for cooperative relaxations of PVDF segments (black bar) and PMMA segments (white bar). For clarity, black and white bars are indicated by arrows in Figure 17A−D. At a sufficiently high temperature (Figure 17A), this length scale is smaller than the average PD of either PVDF (white area) or PMMA (black area) nanoscopic region. Consequently, the relaxations within each region (PVDF, PMMA) in the blend should not differ from those in the corresponding neat polymer. This situation would give rise to two relaxation processes in blends at high temperature, each with the characteristics identical to those observed in the neat polymer. That is indeed what we observe, and it explains why the most probable relaxation time for the α_a process, due to PVDF segments, is independent of blend composition at high temperature (Figure 4). The same is true for the (slower) α_m process in the blends which merges with the α process in neat PMMA at a sufficiently high temperature (see Figure 4), suggesting that the relaxations associated with PMMA segments in a blend are also independent of blend composition at such temperatures. With decreasing temperature, however, the length scale for cooperative relaxation increases and gradually approaches the PD of each nanoscopic region. It is important to realize here that this process occurs at a different rate in PMMA and PVDF regions because, at a given temperature, PMMA segments are inherently less mobile (higher T_g) than PVDF segments. Therefore, the length scale for cooperative relaxations of PMMA segments will increase *faster* with decreasing temperature and will reach the PD of PMMA nanoscopic region *earlier* (i.e., at higher temperature) than in PVDF. From the standpoint of relaxation dynamics, PMMA segments will thus "sense" the presence of the other nanoscopic region (nanohet-

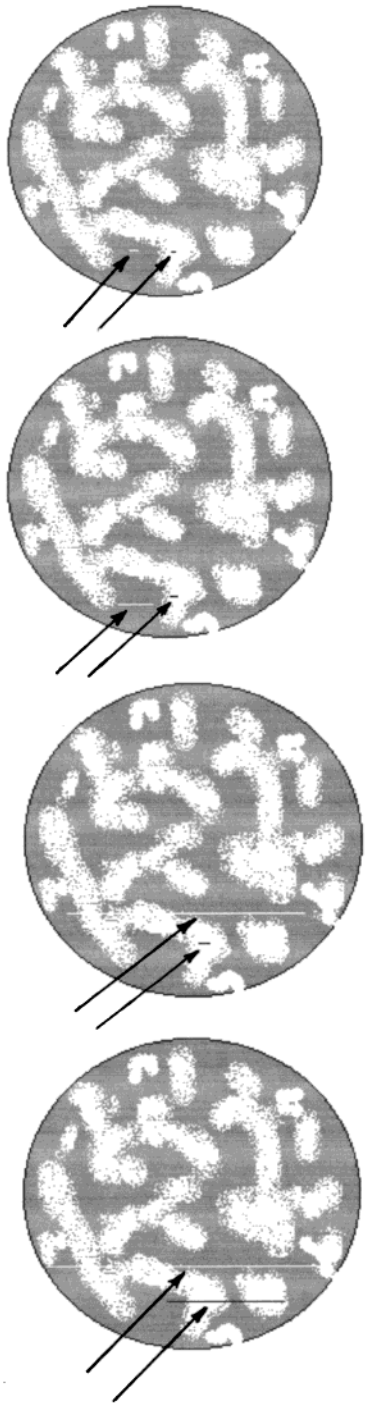

A. Well Above Tg:
Relaxations associated with PVDF and PMMA segments are decoupled. PVDF and PMMA segments relax like in the bulk.

B. Temperature Above Tg:
PMMA segments sense the heterogeneity earlier than PVDF segments. The α_m process shows blend composition dependence and encompasses motions of PMMA and a part of PVDF segments. But other PVDF segments still relax via the α_a process and its dynamics are only slightly affected by the heterogeneity.

C. Temperature Around Tg:
The system is globally vitrified, the segmental motions associated with PMMA segments are frozen and only the β type local motions survive. The α_m to β_m crossover is observed. Relaxations associated with PVDF segments take place in the confined environment since the cooperative length-scale is smaller than the PD of the nanoscopic region. The confinement effect increases as temperature decreases.

D. Temperature Below Tg:
The cooperative length-scale associated with PVDF segments grows and eventually exceeds the PD of the nanoscopic region, at which point their motions are arrested. The large scale rearrangements are preferrably suppressed by the confinement, causing the decrease in most probable relaxation time and the α_a to β_a crossover.

CODE:
Black area: PMMA Segments
White area: PVDF Segments
Black Bar: Cooperative Length-Scale for PVDF Segments
White Bar: Cooperative Length-Scale for PMMA Segments

Figure 17. Schematic for the interplay between the morphology, cooperative length scale, and temperature in PVDF/PMMA blends.

erogeneity) first; this is represented schematically in Figure 17B, where the length scale for cooperative relaxations associated with PMMA segments (white bar, Figure 17B) is now of the order of the PMMA nanoscopic region (black areas, Figure 17B), while the length scale for cooperative relaxations of PVDF segments (black bar, Figure 17B) remains, on average, smaller than the size of the PVDF nanoscopic region (white areas, Figure 17B). This interesting situation gives rise to a gradual emergence of the α_m process, which is composition-dependent and originates in the relaxations that co-involve PMMA segments with a portion of adjacent PVDF segments. Simultaneously, however, the other portion of PVDF segments continues to relax via the α_a process, which is independent of blend composition. A further decrease in temperature leads to the situation

illustrated in Figure 17C: the length scale for cooperative relaxations associated with PMMA segments is now greater than the PD of its nanoscopic region, and the α_m process scales with the overall blend composition in this temperature range (see Figure 10). When this length scale, which continues to increase with decreasing temperature, becomes sufficiently great, the cooperative rearrangements of PMMA segments are arrested, and the system is vitrified; this is manifested by the crossover from α_m to β_m relaxation. As for the PVDF component, as long as the length scale for cooperative relaxations of one portion of PVDF segments remains smaller than the PD of the PVDF nanoscopic region, these segments will continue to relax independently via the α_a process, albeit in an environment *confined* by PMMA. When the length scale for cooperative relaxations of PVDF segments approaches the PD of its nanoscopic region, the role of confinement becomes decisive. At that point relaxations are arrested by geometry (as distinct from temperature), and a crossover from α_a to β_a relaxation is observed. This situation is schematically illustrated in Figure 17D.

In the above scenario, it was implicitly assumed that the systems were wholly amorphous, and no mention was made of the crystalline regions. In crystalline blends, however, the presence of crystalline phase must be taken into account. An important consideration is that the amorphous PVDF segments in blends are confined not only by the rigid PMMA segments but also by the PVDF crystals. The additional confinement notwithstanding, the length scale for relaxation of PVDF segments in crystalline blends at high temperatures is still smaller than the PD of its nanoscopic region, and the relaxation characteristics are the same as in neat PVDF. This explains why the relaxation time for the α_a process at high temperature is independent of degree of crystallinity, as clearly seen in Figures 12 and 15. A decrease in temperature leads to an increase in the length scale for the α_a process and an enhanced probability that these relaxations will be affected by the confinement. An important distinction is how the confinement differs in neat PVDF and in the blends. Because the confinement in blends is contributed by both crystals and rigid PMMA segments, it is expected that the length scale for the α_a process will reach a critical size earlier (at higher temperature) in a blend than in neat PVDF. A manifestation of the confinement effect is a preferable suppression of relaxations associated with larger scale motions within the PVDF nanoscopic region. The size of the confined PVDF domain (where the α_a process originates) is affected by the interlamellar thickness in neat PVDF and by the PD of the nanoscopic region in a blend, which, in turn, is a function of blend composition. An increase in the amount of PMMA in a blend (located within the interlamellar region) will effectively decrease the PD of PVDF nanoscopic region and trigger an earlier (i.e., higher temperature) α_a to β_a crossover; this is evident by inspection of region II in Figure 4.

To advance this argument further, we examine the most probable relaxation time and the relaxation strength of the α_a process as a function of temperature for a wholly amorphous and a crystalline sample. We first compare the temperature dependence of frequency at maximum loss, f_{max}, for quenched and crystalline 60/40 blends. Data for wholly amorphous (filled diamonds) and crystalline (filled circles) sample are presented in Figure 18 (right ordinate). The wholly amorphous sample was prepared by quenching, and the crystalline sample was obtained by subsequent cold crystallization at 57 °C for 24 h. Similar to the trend shown in Figure 4, data fall on top of each other at high temperature, diverge as the temperature is decreased, and eventually cross over to the glassy state (β relaxation) at low temperature. A crossover in the wholly amorphous sample proves that the crossover observed in crystalline blends (see Figure 4) cannot be attributed exclusively to the interphase present in crystalline blends. Furthermore, it was found that the data for the wholly amorphous 60/40 blend (full diamonds, Figure 18) were very similar to those for a fully crystallized 80/20 blend (open triangles, Figure 4). This is an important observation that suggests a key role for the composition of the amorphous phase in determining the α_a to β_a crossover. The PD of PVDF nanoscopic region is smaller than the interlamellar thickness, and consequently, the effect of confinement due to rigid PMMA domains on the α_a process is more pronounced than that of the PVDF crystals.

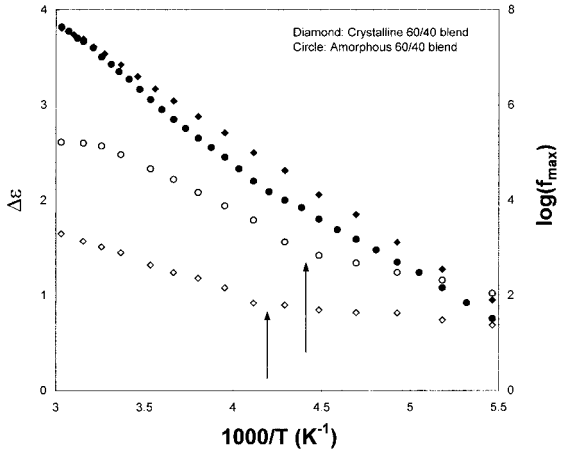

Figure 18. Frequency at loss maximum (right) and relaxation strength (left) as a function of reciprocal temperature for wholly amorphous and crystalline 60/40 blend.

Further insight into α_a to β_a crossover can be gained by monitoring the relaxation strength through the crossover region. In Figure 18 we plot dielectric relaxation strength ($\Delta\epsilon$, left ordinate) as a function of reciprocal temperature for the crystalline (open diamonds) and amorphous (open circles) 60/40 blend. Note that the dielectric strength is more sensitive to the crossover than the relaxation time (solid diamonds and circles), as evidenced by a noticeable change in the temperature dependence of $\Delta\epsilon$ in the crossover range (see arrow in Figure 18). A relatively weak temperature dependence of $\Delta\epsilon$ is observed in both blends at low temperature, where relaxations occur via the β_a process. Following the crossover, $\Delta\epsilon$ increases with increasing temperature. The abrupt increase in the slope is a clear indication that the crossover represents a transition associated with the PVDF nanoscopic region, where segmental motions are now unlocked and act to relax the overall dipole moment. This behavior is interpreted as a manifestation of the effect of confinement and is common to crystalline polymers. An interesting feature of Figure 18 is the continuing increase in relaxation strength with increasing temperature, which is in contrast with the trend that follows the $\alpha_m-\beta_m$ crossover in neat PMMA and a wholly amorphous 50/50 blend (see Figure 11). There are three major differences in the

dielectric response of the crystalline and the wholly amorphous sample of Figure 18: (1) $\Delta\epsilon$ is lower in the crystalline sample, (2) the α_a to β_a crossover is smoother in the crystalline sample, and (3) the glassy state in the crystalline sample extends to a higher temperature, as evidenced by the increase in temperature at which the temperature dependence of $\Delta\epsilon$ changes. The first point is readily understood and is a direct consequence of the decrease in the amount of amorphous PVDF after crystallization. The second and the third difference have the common origin in sense that the confinement effect becomes more pronounced after crystallization and is enhanced by decreasing temperature. Segmental motions within the PVDF nanoscopic region are arrested by geometry at higher temperature in crystalline than in amorphous sample.

Conclusions

We have completed a comprehensive DRS study of the reorientational dynamics of dipoles in PVDF/PMMA blends over 11 decades of frequency. Various systems were investigated including wholly amorphous blends, crystalline blends, and blends undergoing in-situ crystallization. A single calorimetric (DSC) glass transition, observed in all blends, disguises a complex relaxation picture on the nanoscopic level. The principal conclusions are recapped as follows. The α_a process is associated with relaxations of PVDF segments within the nanoscopic amorphous regions of this component. This process cannot be attributed exclusively to the crystalline−amorphous interphase because it is present in crystalline *and* amorphous blends alike. The dynamics of the α_a process are governed by the physical dimension (PD) of PVDF nanoscopic regions and by the length scale for cooperative relaxations of PVDF segments. At sufficiently high temperature, the PD of PVDF regions is greater than the length scale for segmental motions, and the most probable relaxation time is independent of blend composition. With decreasing temperature, however, the length scale for segmental motions becomes commensurate with the PD of nanoscopic regions, and the relaxations become governed by the confinement, which is imposed by rigid PMMA segments and lamellar crystals and which varies with blend composition. The effect of confinement increases with decreasing amount of PVDF in a blend, which results in a decrease in the PD of PVDF nanoscopic regions. This further leads to a decrease in the most probable relaxation time for the α_a process, owing to a preferential suppression of large-scale motions of PVDF segments. A direct consequence of the effect of confinement on relaxation dynamics is the crossover (α_a to β_a) from segmental to localized motions observed in all blends. The α_m (slower) process emerges during cooling from above the melting point. The α_m process depends on blend composition, and it encompasses relaxations in PMMA (α and β) and in the adjacent portion of PVDF segments that are not involved in the α_a process. When the length scale for relaxations via the α_m process, which also decreases with decreasing temperature, becomes sufficiently great, the system undergoes vitrification.

Acknowledgment. This material is based in part on work supported by the National Science Foundation under Grant DMR-9710480.

References and Notes

(1) Wang, T. T.; Nishi, T. *Macromolecules* **1977**, *10*, 421.
(2) Wendorff, J. *J. Polym. Sci., Polym. Lett. Ed.* **1980**, *18*, 439.
(3) Noland, J. S.; Hsu, N. N.-C.; Saxon, R.; Schmitt. J. M. *Adv. Chem. Ser.* **1971**, *99*, 15.
(4) Hourston, D. J.; Hughes, I. D. *Polymer* **1977**, *18*, 1175.
(5) Morra, B. S.; Stein, R. S. *Polym. Eng. Sci.* **1984**, *24*, 311.
(6) Saito, H.; Fujita, Y.; Inoue, T. *Polym. J.* **1987**, *19*, 405.
(7) Douglass, D. C.; McBrierty, V. J. *Macromolecules* **1978**, *11*, 766.
(8) Morra, B. S. Ph.D. Thesis, University of Massachusetts at Amherst, Massachusetts, 1980.
(9) Ullmann, W.; Wendorff, J. H. *Compos. Sci. Technol.* **1985**, *23*, 97.
(10) Hahn, B. R.; Herrmann-Schönherr, O.; Wendorff, J. H. *Polymer* **1987**, *28*, 201.
(11) Saito, H.; Stühn, B. *Macromolecules* **1994**, *27*, 216.
(12) Paul, D. R.; Altamirano, J. O. *Adv. Chem. Ser.* **1975**, *142*, 371.
(13) Mijovic, J.; Han, C. D.; Luo, H. *Polym. Eng. Sci.* **1982**, *22*, 234.
(14) Coleman, M. M.; Zarian, J.; Varnell, D. F.; Painter, P. C. *J. Polym. Sci., Polym. Lett. Ed.* **1977**, *15*, 745.
(15) Roerdink, E.; Challa, G. *Polymer* **1980**, *21*, 509.
(16) Hadziioannou, G.; Stein, R. S. *Macromolecules* **1984**, *17*, 567.
(17) Hahn, B.; Wendorff, J.; Yoon, D. Y. *Macromolecules* **1985**, *18*, 718.
(18) Mijovic, J.; Sy, J.; Kwei, T. K. *Marcromolecules* **1997**, *30*, 3024.
(19) Bernstein, R. E.; Cruz, C. A.; Paul, D. R.; Barlow, J. W. *Macromolecules* **1977**, *10*, 681.
(20) Nishi, T.; Wang, T. T. *Macromolecules* **1975**, *8*, 909.
(21) Di Paola-Baranyi, G.; Fletcher, S. J.; Degre, P. *Macromolecules* **1982**, *15*, 885.
(22) Hudson, S. D.; Davis, D. D.; Lovinger, A. J. *Macromolecules* **1992**, *25*, 1759.
(23) Flory, P. J. *J. Chem. Phys.* **1949**, *17*, 223.
(24) Flory, P. J. *J. Am. Chem. Soc.* **1962**, *84*, 2857.
(25) Mansfield, M. L. *Macromolecules* **1983**, *16*, 914.
(26) Flory, P. J.; Yoon, D. Y.; Dill, K. A. *Macromolecules* **1984**, *17*, 862.
(27) Marqusee, J. A. *Macromolecules* **1989**, *22*, 472.
(28) Mandelkern, L.; Alamo, R. G.; Kennedy, M. A. *Macromolecules* **1990**, *23*, 4721.
(29) Kitamaru, R.; Horil, F.; Hyon, S.-H. *J. Polym. Sci., Polym. Phys. Ed.* **1977**, 15,
(30) Yoon, D. Y.; Flory, P. J. *Macromolecules* **1984**, *17*, 968.
(31) Kumar, S. K.; Yoon, D. Y. *Macromolecules* **1989**, *22*, 4098.
(32) Russell, T. P.; Ito, H.; Wignall, G. D. *Macromolecules* **1988**, *21*, 1703.
(33) Rellick, G. S.; Runt, J. *J. Polym. Sci., Polym. Phys. Ed.* **1986**, *24*, 279.
(34) Runt, J.; Barron, C. A.; Zhang, X.; Kumar, S. K. *Macromolecules* **1991**, *24*, 3466.
(35) Roland, C. M.; Ngai, K. L. *Macromolecules* **1991**, *24*, 2261.
(36) Roland, C. M.; Ngai, K. L. *Macromolecules* **1992**, *25*, 363.
(37) Katana, G.; Fischer, E. W.; Hack, Th.; Abetz, V.; Kremer, F. *Macromolecules* **1995**, *28*, 2714.
(38) Zetsche, A.; Kremer, F.; Jung, H.; Schultze, H. *Polymer* **1990**, *31*, 1988.
(39) Anstasiadis, S. H.; Fytas, G.; Vogt, S.; Gerharz, B.; Fischer, E. W. *Europhys. Lett.* **1993**, *22*, 619.
(40) Shears, M. F.; Williams, G. *J. Chem. Soc., Faraday Trans.* **1973**, *69*, 608.
(41) Ando, Y.; Yoon, D. Y. *Polym. J.* **1992**, *24*, 1329.
(42) Yoon, D. Y.; Ando, Y.; Rozstaczer, S.; Kumar, S. K.; Alfonso, G. C. *Macromol. Chem. Macromol. Symp.* **1991**, *50*, 183.
(43) Kumar, S. K.; Colby, R. H.; Anastasiadis, S. H.; Fytas, G. *J. Chem. Phys.* **1996**, *105*, 3777.
(44) Wetton, R. E.; MacKnight, W. J.; Fried, J. R.; Karasz, F. E. *Macromolecules* **1978**, *11*, 158.
(45) Ando, Y.; Hanada, T.; Saitoh, K. *J. Polym. Sci., Part B: Polym. Phys.* **1993**, 32,
(46) Quan, X.; Johnson, G. E.; Anderson, E. W.; Bates, F. S. *Macromolecules* **1989**, *22*, 2451.
(47) Williams, G. In *Keynote Lectures in Selected Topics of Polymer Science*; Riande, E., Ed.; CSIC: Madrid, 1997; Chapter 1, p 1.
(48) Williams, G. In *Dielectric Spectroscopy of Polymeric Materials: Fundamentals and* Application; Runt, J. P., Fitzgerald, J. J., Eds.; American Chemical Society: Washington, DC, 1997; Chapter 1, p 3.
(49) Simon, G. P. In *Dielectric Spectroscopy of Polymeric Materials: Fundamentals and Application*; Runt, J. P., Fitzgerald, J. J., Eds.; American Chemical Society: Washington, DC, 1997; Chapter 15, p 329.

(50) Williams, G. In *Comprehensive Polymer Science*; Allen, G., Bevington, J. C., Eds.; Pergamon Press: London, 1988; Vol. 2, Chapter 18, pp 601−632.
(51) Williams, G.; Watts, D. C. *Trans. Faraday Soc.* **1970**, *66*, 80.
(52) Dishon, M.; Weiss, G. H.; Bendler, J. T. *J. Res. Natl. Bur. Stand.* **1985**, *90*, 27.
(53) Havrilliak, S.; Negami, S. *J. Polym. Sci., Part C* **1996**, *14*, 99.
(54) Fitz, B.; Andjelic, S.; Mijovic, J. *Macromolecules* **1997**, *30*, 5227.
(55) Andjelic, S.; Mijovic, J. *Macromolecules* **1998**, *31*, 2872.
(56) Nakagawa, K.; Ishida, Y. *J. Polym. Sci., Polym. Phys. Ed.* **1973**, 2153.
(57) Kobayashi, M.; Tashiro, K.; Tadokoro, H. *Marcromolecules* **1975**, *8*, 158.
(58) McCrum, N. G.; Read, B.; Williams, G. *Anelastic and Dielectric Effects in Polymeric Solids;* Wiley: New York, 1967.
(59) Ishida, Y.; Watanabe, M.; Yamafuji, K. *Kolloid-Z.* **1964**, *200*, 48.
(60) Peterlin, A.; Holbrook, J. D. *Kolloid-Z.* **1965**, *203*, 68.
(61) Sasabe, H.; Saito, S.; Asahina, M.; Kakutani, H. *J. Polym. Sci., Part A-2*, **1969**, *7*, 1405.
(62) Nakagawa, K.; Ishida, Y. *J. Polym. Sci., Polym. Phys. Ed.* **1973**, *11*, 1503.
(63) Hirschinger, J.; Schaefer, D.; Spiess, H. W.; Lovinger, A. J. *Macromolecules* **1991**, *24*, 2428.
(64) Miyamoto, Y.; Miyaji, H.; Asai, K. *J. Polym. Sci., Polym. Phys. Ed.* **1980**, *18*, 579.
(65) Karasawa, N.; Goddard, W. A., III. *Macromolecules* **1995**, *28*, 6765.
(66) Massalska-Arodz, M.; Williams. G.; Smith, I. K.; Conolly, C.; Aldridge, G. A.; Dabrowski, R. *J. Chem. Soc., Faraday Trans.* **1998**, *94* (3), 387.
(67) Kwei, T. K.; Nishi, T.; Roberts, R. F. *Macromolecules* **1974**, *7*, 667.
(68) Schmidt-Rohr, K.; Clauss, J.; Spiess, H. W. *Macromolecules* **1992**, *25*, 3273.
(69) Fischer, E. W.; Zetsche, A. *Polym. Prepr. (Am. Chem. Soc., Div. Polym. Chem.)* **1992**, *33*, 78.
(70) Khokhlov, A. R.; Erukhimovich, I. Y. *Macromolecules* **1993**, *26*, 7195.

MA9907035